Research article

Enhancement of electrochemical detection performance towards 2,4,6-trinitrotoluene by a bottom layer of ZnO nanorod arrays

Sanghyeon Moon [a], JeongEun Yoo [a,**], Wonjoo Lee [b,***], Kiyoung Lee [a,*]

[a] *Department of Chemistry and Chemical Engineering, Inha University, 100 Inha-ro, Michuhol-gu, Incheon, 22212, Republic of Korea*
[b] *Aerospace and Defence Reliability Center, Korea Testing Laboratory, 10 Chungui-ro, Jinju-si, Gyeongsangnam-do, 52852, Republic of Korea*

A R T I C L E   I N F O

A B S T R A C T

The ZnO nanostructure layers have been widely investigated as electrodes for sensors due to their intrinsic advantages such as high active area and low cost. In this work, to enhance the detection properties of ZnO nanostructural electrodes, self-organized ZnO nanorod arrays were synthesized using the chemical bath deposition (CBD) method on FTO glasses and ZnO nanoparticles. The fabricated ZnO electrodes on the two different substrates were characterized by SEM, TEM, XRD, and XPS. Subsequently, the detection performance of ZnO nanorod electrodes was electrochemically measured in a 2,4,6-trinitrotoluene (2,4,6-TNT) solution by CV and EIS. The differences in current densities between the ZnO electrodes were determined by the width of the ZnO nanorods, resulting in a ~45% higher detection efficiency with F-CBD (the ZnO nanorods on FTO) electrodes compared to S-CBD (the ZnO nanorods on ZnO nanoparticles) electrodes.

1. Introduction

Explosives have been applied in the wide-field of industry, such as mining, demolition, and military activities [1–3]. However, explosive compounds, such as the major explosive nitro-compounds that decompose into toxic amine-compounds of 2,4,6-trinitrotoluene (2,4,6-TNT), 2,4-dinitrotoluene, octogen, hexogen, and picric acid, are harmful to the environment as they can permeate into underground water [2]. Moreover, explosives have been used for terrorist activities for several decades. Thus, detecting explosive compounds is crucial, not only to identify pollutants but also to trace terrorism activities. To detect the explosive compounds, chromatographic and spectrometric analysis including high-performance liquid chromatography [4], gas chromatography [5], mass spectrometry [6], and ion mobility spectrometry [7] have been utilized to verify the presence of explosive compounds. Among these methods, electrochemical detection techniques are applied for a portable explosive sensor due to its rapid response, convenient operation, and high reproducibility [1,2]. As an electrode for the electrochemical sensors, generally carbon-based electrodes with noble metals are used [8]. However, recently, lots of researcher have investigated metal-oxide-based nanostructure electrodes to avoid using noble metals and obtain economic benefits [9]. In particular, ZnO is one of the reliable materials, allowing detection of the major explosive nitro-compounds. To fabricate ZnO, numerous techniques have been investigated, such as, thermal evaporation [10], metal organic chemical-vapor-deposition [11], and chemical bath-deposition (CBD) method [12]. In this study, CBD method, the one of the

---

simple and facile processes was constructed to grow ZnO nanorod arrays [1]. Through the CBD method, two distinct geometric of ZnO nanorods were obtained on different types of bottom layers. After that, the ZnO nanorod layers were applied to electrochemical detection of 2,4,6-TNT by cyclic voltammetry (CV) technique in an aqueous solution.

2. Experimental

2.1. Fabrication of ZnO electrodes

To obtain two different types of ZnO nanorod electrodes, fluorine-doped tin oxide (FTO) and ZnO nanoparticle coated FTO glasses were prepared as substrates. First, FTO glass was cut into 2 × 6 cm. The cut FTO glasses were ultrasonically cleaned by acetone, ethanol, and deionized water for 5 min. All the cleaned glasses were dried by nitrogen stream. The spin-coating method was applied to deposit the ZnO nanoparticle seed layer onto the FTO surface. A 0.4 mL of ZnO nanoparticle dispersed solution (50–80 nm; US Research Nanomaterials, Inc.) was dropped on the FTO surface; the sample was rotated at 1,000 rpm for 30 s followed by 3,000 rpm for 30 s. The seed-layer-deposited FTO sample was dried in the convection oven and air atmosphere at 60 °C for 2 min.

CBD method was utilized to fabricate the ZnO nanorod arrays on the two different types of oxide layer's surface: the cleaned FTO (denoted as 'F-CBD') and the seed-layer-deposited FTO (denoted as 'S-CBD'). 0.05 M of zinc nitrate hexahydrate (ZNH; reagent grade with 98%, Sigma-Aldrich) and hexamethylenetetramine (HMT; ACS reagent ≥99.0%, Sigma-Aldrich) were mixed in 500 mL of deionized water. The prepared two-different substrates were immersed in the solution at 70 °C for 48 h [12]. After the CBD process, all samples were rinsed by deionized water and annealed at 400 °C in air for 30 min (Scheme 1).

2.2. Characterization of ZnO nanorod electrodes

Field emission scanning microscope (FE-SEM, S-4300, Hitachi) was used to observe the morphological properties of ZnO nanorod electrodes with top views and cross-sectional views (Inha University, Core Facility Center for Sustainable Energy). X-ray diffractometer (XRD, X'pert PRO MRD, Phillips) and field emission transmission electron microscope (FE-TEM, JEM-2100F, JEOL) were employed to analyze the crystallinity and plane distance of the electrodes. Binding energy of elements and element composition of the electrodes were analyzed by X-ray photoelectron spectroscopy (XPS, K-Alpha, Thermo Scientific).
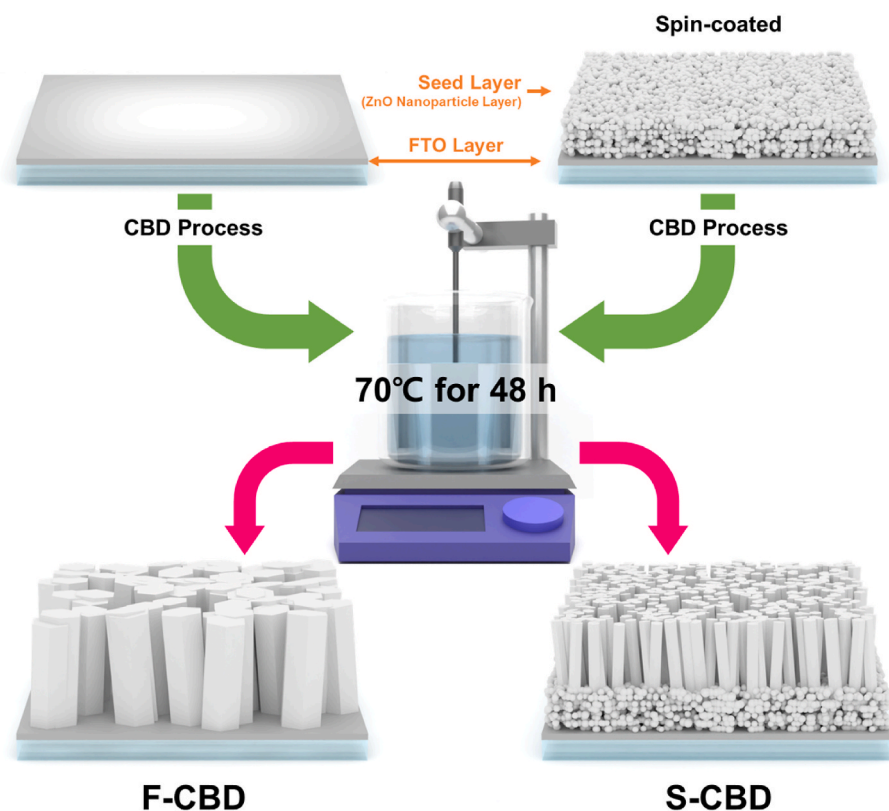
Scheme 1. Schematic diagram of CBD fabricating process for two different types of ZnO nanorod array electrodes: (left) direct-grown on FTO layer; F-CBD and (right) seed-layer-deposited layer; S-CBD.

2.3. Electrochemical analysis

All of electrochemical performance evaluations were conducted in three-electrode system. The three types of electrodes (i.e. pristine FTO, ZnO nanorod arrays directly grown on the FTO and on the seed layer) were utilized as a working electrode; Pt mesh was used as a counter electrode; Ag/AgCl | 3 M KCl was used as a reference electrode. All the electrochemical measurements were progressed by a potentiostat (SP-150 and VSP, Biologic). The difference of redox trace of nitro-compounds and active site density of the three electrodes were investigated by cyclic voltammetry in a 0.1 M of KCl including 100 ppm 2,4,6-TNT. 2,4,6-TNT were fabricated following our previous reports [2]. Where, the potential range was set to −1.3 to 1.3 V (vs. Ag/AgCl, 3 M KCl) with 10 mV s^{-1} of scan rate. The electrochemical impedance spectroscopy (EIS) was investigated at 0 V vs. open-circuit potential with 10 mV amplitude, and the frequency range was set 10^{-2} to 10^4 Hz. All Nyquist plots were fitted to the Randles equivalent circuit.

3. Results and discussion

The synthesis mechanism of ZnO nanorods on the different substrates is described briefly via the following equations [13–15];

$$Zn(NO_3)_2 \bullet 6H_2O \rightarrow Zn^{2+} + 2NO_3^- + 6H_2O \tag{1}$$

$$C_6H_{12}N_4 + 6H_2O \rightarrow 6HCHO + 4NH_3 \tag{2}$$

$$Zn^{2+} + 4NH_3 \rightarrow Zn(NH_3)_4^{2+} \tag{3}$$

$$Zn^{2+} + 4OH^- \rightarrow Zn(OH)_4^{2-} \tag{4}$$

$$Zn(OH)_4^{2-} \rightarrow ZnO + H_2O + 2OH^- \tag{5}$$

$$Zn(NH_3)_4^{2+} + 2OH^- \rightarrow ZnO + 4NH_3 + H_2O \tag{6}$$

According to the equation, zinc nitrate hexahydrate (ZNH) and hexamethylenetetramine (HMT) in the solution provides Zn^{2+} sources (Equation (1)) and NH_3 sources (Equation (2)), respectively. The Zn^{2+} and NH_3 are essential to form zinc-tetraammine ions (Equation (3)) and zinc-hydroxide ion complex (Equation (4)), fabricating solid state of ZnO (Equations 5 and 6). Through the CBD method, the ZnO are precipitated as particles and stacked on the substrates during immersing process.

Fig. 1a indicates the FE-SEM images of 500 nm thick pristine FTO layer on a glass substrate. After CBD process, the FTO substrates were covered with ∼500 nm width and ∼2.3 µm length of ZnO nanorods (F-CBD, Fig. 1b) and ∼100 nm width and ∼1.3 µm length of ZnO nanorods on the 1 µm thick ZnO nanoparticle seed layer (S-CBD, Fig. 1c). As shown Fig. 1b and c, the large grain of FTO provides the larger size of ZnO nanorods (500 nm, F-CBD) and the small grains (∼80 nm, S-CBD) of ZnO nanoparticles formed small size of ZnO
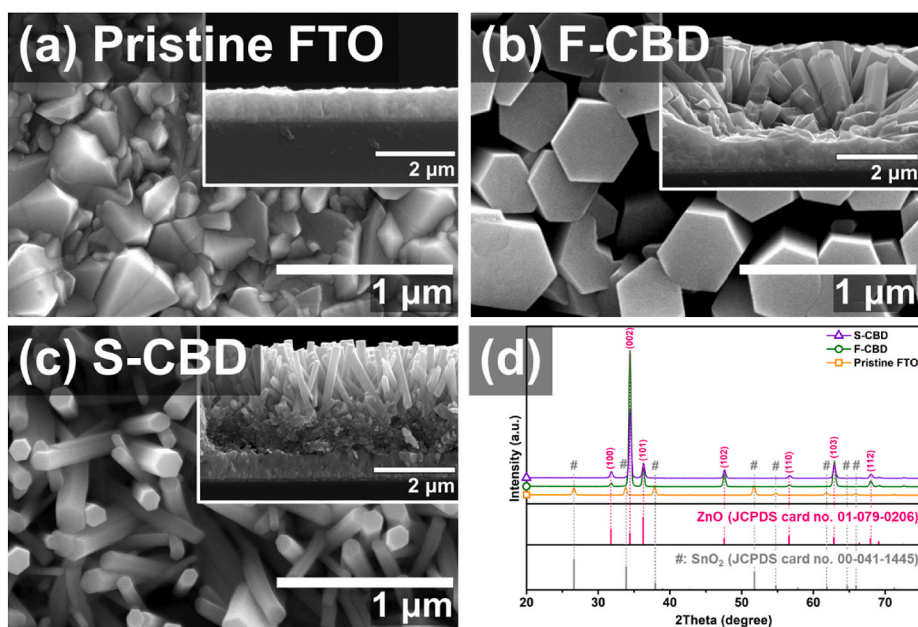

Fig. 1. FE-SEM images of (a) pristine FTO, (b) F-CBD, and (c) S-CBD. Insets show cross-section of the FTO, F-CBD, and S-CBD. (d) XRD patterns of the pristine FTO, F-CBD, and S-CBD electrode.

nanorods (~100 nm). Thus, the results indicate that the width of the ZnO nanorods are dependent on the grain sizes of the substrates. Both ZnO nanorod arrays were grown up to 2.3 μm. The crystalline structures of the electrodes were analyzed by XRD (Fig. 1d). The peaks of F-CBD and S-CBD were appeared at 31.7, 34.4, 36.2, 47.5, 56.6, 62.8, and 67.9° corresponding to (100), (002), (101), (102), (110), (103), and (112) plane of ZnO (JCPDS card number: 01-079-0206). Additionally, the crystallinity of ZnO electrodes were
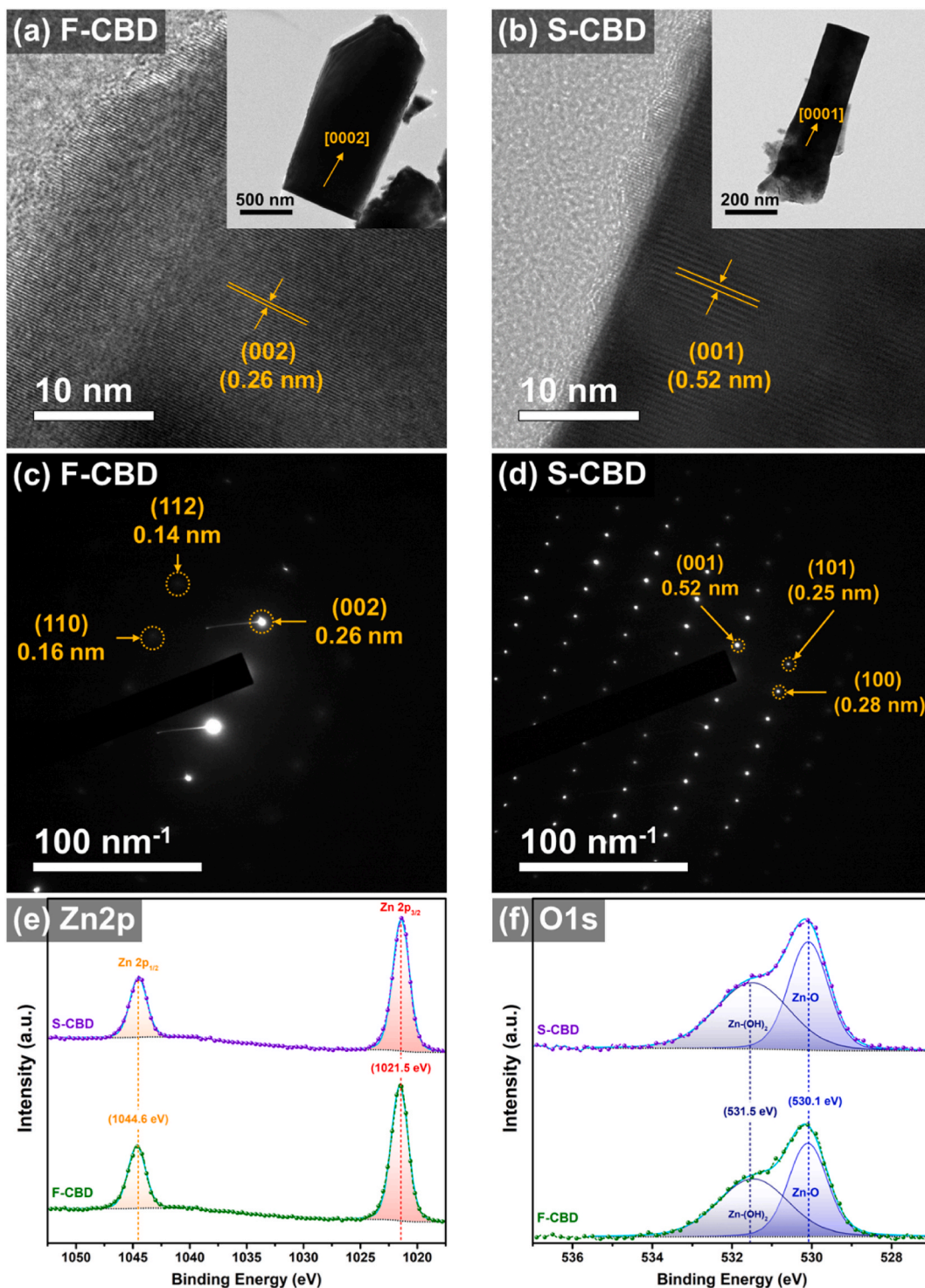

Fig. 2. HR-TEM images of the (a) F-CBD and (b) S-CBD (insets show low-magnification images of the electrodes). SAED patterns of the (c) F-CBD and (d) S-CBD. High-resolution XPS spectra of the F-CBD and S-CBD: (e) Zn2p and (f) O1s.

characterized by high-resolution TEM (Fig. 2a and **b**) and Selected Area Electron Diffraction (SAED) patterns (Fig. 2c and **d**). Inter-planar distances (*d-spacing*) of the ZnO nanorods in Fig. 2 were calculated by Equation (7) and cross-checked by using Bragg's Law (Equation (8)) with XRD patterns of ZnO nanorods in Fig. 1d [1].

$$\lambda_{TEM} L = dr \tag{7}$$

$$n\lambda_{XRD} = 2d \sin \theta \tag{8}$$

where $\lambda_{TEM} L$ is a camera constant (9.25 nm^2), d is *d-spacing* value (nm) of the ZnO nanorods, r is a radius of spot in SAED pattern, n is an order of diffraction (set as '1'), λ_{XRD} is a wavelength of X-ray (Cu kα, 0.15406 nm), and θ is a Bragg angle (°). According to Fig. 2a and **b**, lattice fringes of ~ 0.26 nm and ~ 0.52 nm corresponds to the (002) and (001) plane of hexagonal ZnO structure. It suggests that ZnO nanorod arrays were grown as a [0002] direction (the insets in Fig. 2a and **b**) [13]. Thus, calculated *d-spacing* values from SAED
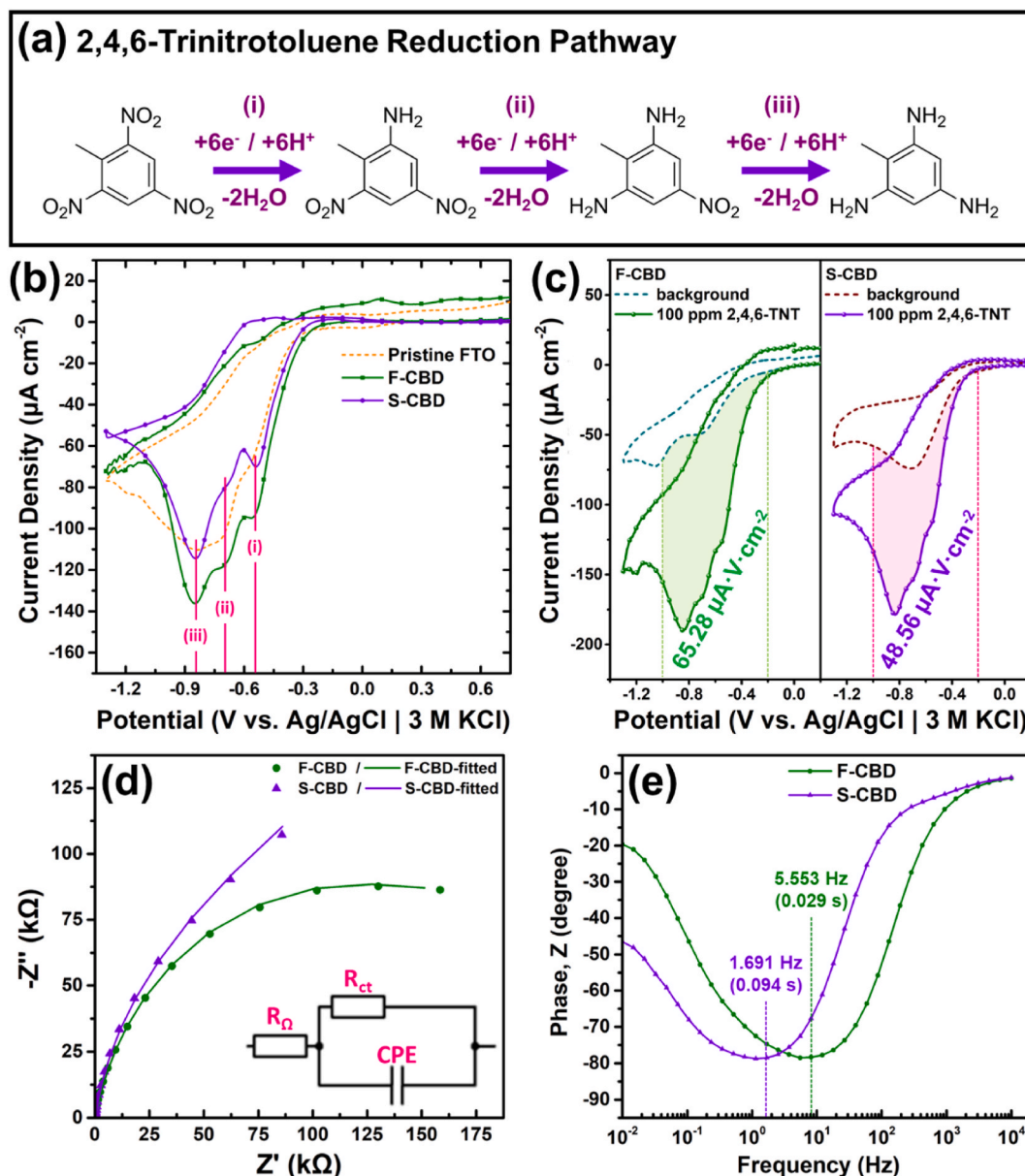

Fig. 3. (a) Electrochemical reduction pathway of 2,4,6-trinitrotoluene. (b) Cyclic voltammograms of 100 ppm 2,4,6-TNT, which was detected with pristine FTO, F-CBD, and S-CBD electrode (background signals were subtracted). (c) Cyclic voltammograms of background signals and detection performance of F-CBD, and S-CBD electrode in 100 ppm of 2,4,6-TNT (background was not subtracted). (d) Nyquist plots and (e) Bode plots of F-CBD and S-CBD; Randle's equivalent circuit was represented in the inset of Fig. 3d.

patterns are consistent with the diffraction peaks of 31.7, 34.4, 36.2, 56.6, and 67.9° in Fig. 1d, indicating that F-CBD and S-CBD were well-crystallized during fabrication. High-resolution XPS spectrum of Zn2p and O1s were additionally analyzed to the ZnO nanorod array electrodes. In Fig. 2e, $Zn2p_{1/2}$ and $Zn2p_{3/2}$ were observed at 1044.6 and 1021.5 eV, corresponding to the Zn^{2+} of ZnO lattice. Moreover, the peaks at 531.5 and 530.1 eV indicate $Zn-(OH)_2$ and $Zn-O$ bonds in the O1s spectra (Fig. 2f). The identical peaks in Fig. 2e and **f** demonstrate that the surface of F-CBD and S-CBD electrodes include the same chemical bonding, consisting of the oxygen and hydroxide with zinc atoms.

The reduction pathway of 2,4,6-TNT in an aqueous medium is displayed in Fig. 3a. Each nitro group is electrochemically reduced to amine group with six electrons and protons [3,16], and the reduction steps are observed as cathodic reduction peaks in a voltammogram. The cyclic voltammograms of the three different types of ZnO electrodes (pristine FTO, F-CBD, and S-CBD) were shown in Fig. 3b. All the voltammograms were subtracted background signals. The voltammograms indicate that all the electrodes can conduct electrochemical detection of 2,4,6-TNT in an aqueous solution as generating the three reduction peaks from −0.4 to −1.0 V. Each reduction peak represents the reduction steps of 2,4,6-TNT as shown in Fig. 3a. Interestingly, current intensity of reduction peaks with FTO and S-CBD electrode is similar. However, in case of FTO electrode result, the peaks are not clear enough to be identified. In contrast, the ZnO nanorod electrodes show three distinct peaks. Furthermore, F-CBD achieved higher current density compared with S-CBD at the voltammogram results, *i.e.* 35.4, 45.9 and 18.9% at the first, second, and third reduction peak respectively. The results indicate that grown ZnO nanorod arrays on FTO substrate allow to enhance the detecting sensitivity of 2,4,6-TNT since Zn and O atoms at the lattice of ZnO act as adsorption sites of the 2,4,6-TNT or other nitro groups. Moreover, the active site density (ASD) was measured and evaluated by Equation (9) [17–20].

$$ASD = \frac{CV\ area \times N}{n \times scan\ rate \times F} \tag{9}$$

where '*CV area*' is a faradaic area between background and analyte-detected signal of CVs, N is the number of Avogadro (6.023×10^{23} active sites · mol^{-1}), n is the number of electrons that used to reduce the 2,4,6-TNT (18 electrons were used in the reduction process), and F is the Faraday constant (96485 $C\ mol^{-1}$). At the equation, '*CV area*' is a key parameter to compare the ASD. As shown in Fig. 3c, ASD of F-CBD was obtained 65.28, which is are 34.43% larger active sites compared with S-CBD (48.56 $\mu A\ V\ cm^{-2}$). Thus, it is concluded that adsorbing performance of 2,4,6-TNT is much higher on the F-CBD surface than on S-CBD. EIS was additionally measured to obtain a correlation with charge transfer resistance, electrochemical reaction time, and detection performance. Nyquist plots in Fig. 3d were fitted to Randle's circuit (inset of the figure): R_Ω is a resistance of electrolyte, R_{ct} is a charge transport resistance, CPE is a constant phase element. The R_{ct} is crucial parameter because it enables to compare an electric conductivity. From Figs. 3d and 213.4 (F-CBD) and 253.9 kΩ (S-CBD) of the R_{ct} obtained, indicating the electric conductivity of the F-CBD is 18.9% higher compared to the S-CBD. The ZnO nanoparticle seed layers acted as a resistance layer and reduce the conductivity. Additionally, electrochemical reaction time (τ) in the Bode plot (Fig. 3e) was calculated by Equation (10) [1],

$$\frac{1}{\omega_{max}} = \frac{1}{2\pi f_{max}} = \tau \tag{10}$$

where the ω_{max} is a maximum angular velocity at a maximum phase angle (f_{max}). The f_{max} of F-CBD and S-CBD was evaluated to 5.553 and 1.691 Hz and the τ was calculated to 0.029 and 0.094 s, respectively. Consequently, the analytes were 224% efficiently detected at the F-CBD's surface compared to at the S-CBD surface. Finally, from EIS results, it is concluded that the 2,4,6-TNT detecting performance of ZnO nanorod electrodes is critically affected by three factors: (1) active site density, (2) electric conductivity, and (3) electrochemical reaction kinetics. Moreover, although the S-CBD has smaller ZnO nanorods than F-CBD (Fig. 1), F-CBD has a larger electrochemical surface area due to better diffusion behavior and additional resistance on the seed layer of S-CBD. This allows F-CBD to provide better detection performance.

4. Conclusion

In the present work, we addressed that the synthesis of self-aligned ZnO nanorod arrays as a detecting electrode for 2,4,6-TNT by CBD method. The SEM images demonstrated that ZnO nanorod arrays were well-grown on two different substrates (pristine FTO and ZnO nanoparticle layer on FTO), and the nanorod width is dependent on the grain sizes of the substrates, i.e. ~500 on the FTO (F-CBD) and ~100 nm on the ZnO nanoparticle seed layer (S-CBD). From CV results, pristine FTO, F-CBD, and S-CBD showed three peaks related to 2,4,6-TNT reduction, however, the peaks of pristine FTO were not clear to be identified and the intensity of S-CBD peaks much smaller than the peaks of F-CBD. The enhancement of detection performance at F-CBD was elucidated by CV and EIS measurements. In the case of ASD, high active site density of F-CBD was measured and calculated, and by Nyquist and bode plot, the low charge transfer resistance, and fast kinetics of electrochemical reaction at electrode surface/electrolyte interface was investigated and evaluated. Consequently, all the electrochemical measurement resulted that the ZnO nanorod arrays directly fabricated on FTO layer for 2,4,6-TNT performed ~45% higher compared with ZnO nanorods on ZnO nanoparticle layers. However, further research must be conducted to improve the detection sensitivity as adjusting the geometry of the ZnO nanorod arrays. Furthemore, the optimized ZnO electrode has to be able to detect not only 2,4,6-TNT but also various explosive analytes (e.g., 2,4,6-dinitrotoluene, octogen, hexogen, picric acid).

Author contribution statement

Sanghyeon Moon: Performed the experiments; Wrote the paper.
JeongEun Yoo: Conceived and designed the experiments; Wrote the paper.
Wonjoo Lee: Conceived and designed the experiments; Contributed reagents, materials, analysis tools or data; Wrote the paper.
Kiyoung Lee: Conceived and designed the experiments; Analyzed and interpreted the data; Wrote the paper.

Data availability statement

Data will be made available on request.

Additional information

No additional information is available for this paper.

Declaration of competing interest

The authors declare that they have no known competing financial interests or personal relationships that could have appeared to influence the work reported in this paper.

Acknowledgement

References

[1] S. Moon, D.K. Charyulu, J. Lee, T. Kim, J. Kim, W. Lee, K. Lee, Chemical-bath-deposited rutile TiO2 film for electrochemical detection of 2,4,6-trinitrotoluene, Thin Solid Films 748 (2022), 139172, https://doi.org/10.1016/j.tsf.2022.139172.
[2] S. Moon, D. Kamakshaiah Charyulu, W. Lee, K. Lee, Controlling the geometric design of anodic 1D TiO2 nanotubes for the electrochemical reduction of 2,4,6-trinitrotoluene in ambient conditions, J. Electroanal. Chem. 900 (2021), 115717, https://doi.org/10.1016/j.jelechem.2021.115717.
[3] A. Dettlaff, P. Jakobczyk, M. Ficek, B. Wilk, M. Szala, J. Wojtas, T. Ossowski, R. Bogdanowicz, Electrochemical determination of nitroaromatic explosives at boron-doped diamond/graphene nanowall electrodes: 2,4,6-trinitrotoluene and 2,4,6-trinitroanisole in liquid effluents, J. Hazard Mater. 387 (2020), 121672, https://doi.org/10.1016/j.jhazmat.2019.121672.
[4] T.D. Schachel, A. Stork, R. Schulte-Ladbeck, T. Vielhaber, U. Karst, Identification and differentiation of commercial and military explosives via high performance liquid chromatography - high resolution mass spectrometry (HPLC-HRMS), X-ray diffractometry (XRD) and X-ray fluorescence spectroscopy (XRF): towards a forensic substance database on explosives, Forensic Sci. Int. 308 (2020), 110180, https://doi.org/10.1016/j.forsciint.2020.110180.
[5] M. Hariri, K. Ghani, S. Damiri, Purification of 2,4,6-trinitrotoluene by digestion with sodium sulfite and determination of its impurities by gas chromatography–electron capture detector (GC-ECD), J. Iran. Chem. Soc. 16 (11) (2019) 2401–2408, https://doi.org/10.1007/s13738-019-01709-z.
[6] C.E. Son, S.S. Choi, Deprotonation of trinitrotoluene in atmospheric pressure chemical ionization mass spectrometry, Rapid Commun. Mass Spectrom. 37 (3) (2023), e9434, https://doi.org/10.1002/rcm.9434.
[7] N. Jurado-Campos, U. Chiluwal, G.A. Eiceman, Improved selectivity for the determination of trinitrotoluene through reactive stage tandem ion mobility spectrometry and a quantitative measure of source-based suppression of ionization, Talanta 226 (2021), 121944, https://doi.org/10.1016/j.talanta.2020.121944.
[8] B. Filanovsky, B. Markovsky, T. Bourenko, N. Perkas, R. Persky, A. Gedanken, D. Aurbach, Carbon electrodes modified with TiO2/metal nanoparticles and their application for the detection of trinitrotoluene, Adv. Funct. Mater. 17 (9) (2007) 1487–1492, https://doi.org/10.1002/adfm.200600714.
[9] S. Moon, S.S. Patil, S. Yu, W. Lee, K. Lee, Electrochemical characteristic assessments toward 2,4,6-trinitrotoluene using anodic TiO2 nanotube arrays, Electrochem. Commun. 135 (2022), 107214, https://doi.org/10.1016/j.elecom.2022.107214.
[10] K.M.K. Srivatsa, D. Chhikara, M.S. Kumar, Synthesis of aligned ZnO nanorod array on silicon and sapphire substrates by thermal evaporation technique, J. Mater. Sci. Technol. 27 (8) (2011) 701–706, https://doi.org/10.1016/s1005-0302(11)60129-1.
[11] Q. Hao, Improved manufacturing processes for better materials properties — from quantum dots to bulk materials, ES Mater. Manuf. 8 (2020) 1–2, https://doi.org/10.30919/esmm5f765.
[12] W. Lee, S.K. Min, V. Dhas, S.B. Ogale, S.-H. Han, Chemical bath deposition of CdS quantum dots on vertically aligned ZnO nanorods for quantum dots-sensitized solar cells, Electrochem. Commun. 11 (1) (2009) 103–106, https://doi.org/10.1016/j.elecom.2008.10.042.
[13] Y. Qu, X. Huang, Y. Li, G. Lin, B. Guo, D. Song, Q. Cheng, Chemical bath deposition produced ZnO nanorod arrays as an antireflective layer in the polycrystalline Si solar cells, J. Alloys Compd. 698 (2017) 719–724, https://doi.org/10.1016/j.jallcom.2016.12.265.
[14] A. Qurashi, M. Faiz, N. Tabet, M.W. Alam, Low temperature synthesis of hexagonal ZnO nanorods and their hydrogen sensing properties, Superlattice. Microst. 50 (2) (2011) 173–180, https://doi.org/10.1016/j.spmi.2011.05.014.
[15] L.L. Yang, Q.X. Zhao, M. Willander, Size-controlled growth of well-aligned ZnO nanorod arrays with two-step chemical bath deposition method, J. Alloys Compd. 469 (1–2) (2009) 623–629, https://doi.org/10.1016/j.jallcom.2008.08.002.
[16] C.K. Chua, M. Pumera, L. Rulíšek, Reduction pathways of 2,4,6-trinitrotoluene: an electrochemical and theoretical study, J. Phys. Chem. C 116 (6) (2012) 4243–4251, https://doi.org/10.1021/jp209631x.
[17] S. Alnemrat, G.T. Brett, J.P. Hooper, Adsorption of 2,4,6-trinitrotoluene on the ZnO (21̄1̄0) surface: a density functional theory study of the detection mechanism of ZnO nanowire chemiresistors, Appl. Phys. Lett. 103 (17) (2013), 173102, https://doi.org/10.1063/1.4825365.
[18] M. Breedon, M.J.S. Spencer, I. Yarovsky, Adsorption of NO2 on oxygen deficient ZnO(21̄1̄0) for gas sensing applications: a DFT study, J. Phys. Chem. C 114 (39) (2010) 16603–16610, https://doi.org/10.1021/jp105733p.
[19] P.S. Maddahi, N. Shahtahmassebi, M. Rezaee Roknabadi, F. Moosavi, Exploring the sensitivity of ZnO nanotubes to tyrosine nitration: a DFT approach, Phys. Lett. 380 (24) (2016) 2090–2097, https://doi.org/10.1016/j.physleta.2016.04.013.
[20] T. Zhang, P. Wojtal, O. Rubel, I. Zhitomirsky, Density functional theory and experimental studies of caffeic acid adsorption on zinc oxide and titanium dioxide nanoparticles, RSC Adv. 5 (129) (2015) 106877–106885, https://doi.org/10.1039/c5ra21511k.